



Detection of 36 GHz Class I Methanol Maser Emission toward NGC 4945

Tiege P McCarthy^{1,2}, Simon P. Ellingsen¹, Xi Chen^{3,4}, Shari L. Breen⁵, Maxim A. Voronkov², and Hai-hua Qiao^{3,6}

¹School of Physical Sciences, University of Tasmania, Hobart, TAS 7001, Australia; tiegem@utas.edu.au

²Australia Telescope National Facility, CSIRO, P.O. Box 76, Epping, NSW 1710, Australia

³Center for Astrophysics, GuangZhou University, Guangzhou 510006, China

⁴Shanghai Astronomical Observatory, Chinese Academy of Sciences, Shanghai 200030, China

⁵Sydney Institute for Astronomy (SfA), School of Physics, University of Sydney, Sydney, NSW 2006, Australia

⁶National Time Service Center, Chinese Academy of Sciences, Xi'An, Shaanxi 710600, China

Received 2017 July 5; revised 2017 August 2; accepted 2017 August 17; published 2017 September 13

Abstract

We have searched for emission from the 36.2 GHz ($4_{-1} \rightarrow 3_0E$) methanol transition toward NGC 4945, using the Australia Telescope Compact Array. 36.2 GHz methanol emission was detected offset southeast from the Galactic nucleus. The methanol emission is narrow, with a line width $< 10 \text{ km s}^{-1}$ and a luminosity five orders of magnitude higher than Galactic class I masers from the same transition. These characteristics combined with the physical separation from the strong central thermal emission suggests that the methanol emission is a maser. This emission is a factor of ~ 90 more luminous than the widespread emission detected from the Milky Way central molecular zone. This is the fourth detection of extragalactic class I emission and the third detection of extragalactic 36.2 GHz maser emission. These extragalactic class I methanol masers do not appear to be simply highly luminous variants of Galactic class I emission and instead appear to trace large-scale regions of low-velocity shocks in molecular gas, which may precede, or be associated with, the early stages of large-scale star formation.

Key words: masers – galaxies: individual (NGC 4945) – galaxies: starburst – radio lines: ISM

1. Introduction

Methanol maser emission is a commonly observed phenomenon in the Milky Way. The species has a rich spectrum of masing transitions, allowing it to be utilized as a powerful tool for probing high-mass star formation regions in our Galaxy. Galactic methanol masers have now been detected in more than 1200 sources (e.g., Ellingsen et al. 2005; Caswell et al. 2010, 2011; Green et al. 2010, 2012, 2017; Voronkov et al. 2014; Breen et al. 2015). The masing transitions of methanol are empirically divided into two classes, based on the pumping mechanism responsible for excitation, collisional for class I and radiative for class II. Galactic class I masers are typically associated with the interaction of shocked gas with molecular clouds, driven by outflows or expanding H II regions (Kurtz et al. 2004; Cyganowski et al. 2009, 2012; Voronkov et al. 2010, 2014). These shocks aid the release of methanol into the gas phase, along with warming and compressing the gas, which produces optimal masing conditions (Voronkov et al. 2010). Class I masers are often observed distributed across many different sites within one star formation region, on scales up to 1 pc (Voronkov et al. 2014). Galactic class II masers are closely associated with young stellar objects (YSOs), which are often accompanied by OH and H₂O masers, and are usually observed in one or two compact sites within a star formation region (e.g., Ellingsen 2006; Breen et al. 2010; Caswell et al. 2010). Class II masers are exclusively observed toward high-mass star formation regions (Breen et al. 2013), while class I masers have been observed associated toward low- and high-mass star formation regions as well as supernova remnants (e.g., Kalenskii et al. 2010; Pihlström et al. 2014).

Despite the abundance of masing methanol observed within our Galaxy, extragalactic methanol masers are a rarely observed phenomena. Class II maser emission (either 6.7 or 12.2 GHz) has been observed in the Large Magellanic Cloud and M31, with what appear to be similar properties to their

Galactic counterparts (Green et al. 2008; Ellingsen et al. 2010; Sjouwerman et al. 2010). Extragalactic class I emission has been previously observed at 36.2 GHz in NGC 253 and Arp 220 (Ellingsen et al. 2014; Chen et al. 2015), and in NGC 1068 at 84.5 GHz (Wang et al. 2014). Two of these reported extragalactic class I sources (Arp 220 and NGC 1068) are luminous enough to be considered megamasers ($> 10 L_{\odot}$). In contrast to the extragalactic class II masers, these class I sources do not appear to be the result of similar processes as their Galactic equivalents; instead, they appear to trace regions of large-scale molecular infall (Ellingsen et al. 2017b).

The 36.2 GHz $4_{-1} \rightarrow 3_0E$ methanol transition is one of the most common class I methanol masers observed toward star formation regions in the Milky Way (Haschick & Baan 1989; Voronkov et al. 2014). Widespread emission from this same transition has also been observed in the inner region of our Galaxy, with over 350 independent sites detected within a $160 \times 43 \text{ pc}$ region resulting in an integrated luminosity $> 5600 \text{ Jy km s}^{-1}$ (Yusef-Zadeh et al. 2013). Photodesorption of methanol from cold dust by cosmic rays has been suggested as the mechanism producing the abundance of methanol required to produce these levels of observed methanol maser emission (Yusef-Zadeh et al. 2013). It is reasonable to expect that a similar phenomenon may exist in other other galaxies, with Ellingsen et al. (2014) suggesting that galaxies with enhanced star formation may display this emission over even larger volumes, making them more readily detectable.

Here, we report a search for the class I 36.2 GHz and class II 37.7 GHz transitions toward the central region of NGC 4945. This nearby (assumed distance of $3.7 \pm 0.3 \text{ Mpc}$; Tully et al. 2013) galaxy is classified as a barred-spiral and starburst type. In addition to being classified as a starburst, the nucleus of NGC 4945 is also classified as an active galactic nucleus (AGN) and is the strongest source of hard X-rays observed from Earth (Done et al. 1996). Analysis of near- and far-infrared observations indicates that the AGN is heavily

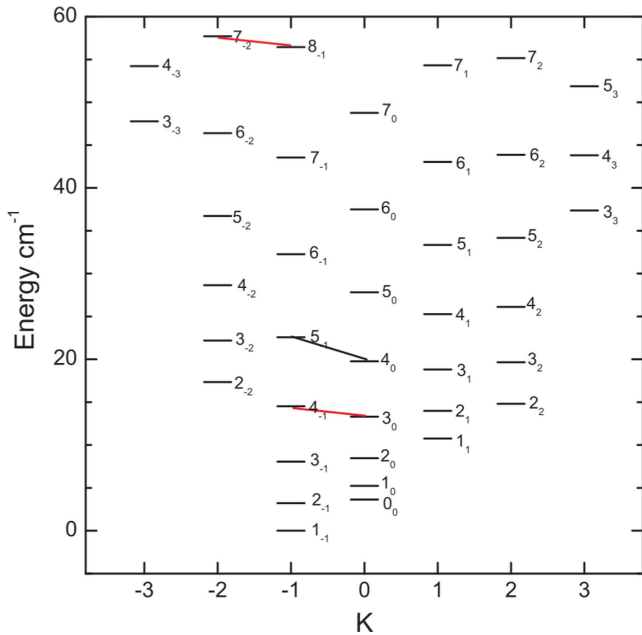


Figure 1. Rotational energy level diagram for E-type methanol originally presented in Chen et al. (2015) and based on the CDMS catalog (Müller et al. 2001). The three marked transitions correspond to the transitions of class I methanol observed masing in extragalactic sources (Ellingsen et al. 2014; Wang et al. 2014; Chen et al. 2015). The red marked transitions are those searched for toward NGC 4945, NGC 253, and Arp 220, with the black marked transition representing the 84.5 GHz transition detected in NGC 1068 (Wang et al. 2014).

obscured and that the starburst process is the primary source of energy for exciting photoionized gas (Marconi et al. 2000; Spoon et al. 2000, 2003; Pérez-Beaupuits et al. 2011). NGC 4945 has a star formation rate of $4.35 \pm 0.25 M_{\odot} \text{ yr}^{-1}$ (Bendo et al. 2016), almost a factor of three more than the $1.65 \pm 0.19 M_{\odot} \text{ yr}^{-1}$ observed in the Milky Way (Licquia & Newman 2015).

2. Observations

The observations were made using the Australia Telescope Compact Array (ATCA) on 2015 August 25 and 26 (project code C2879). The observations utilized the EW352 array, with minimum and maximum baselines of 31 and 352 m resulting in a synthesized beam of approximately 26×4 arcsec at 36.2 GHz (elongation caused by limited hour-angle coverage). The Compact Array Broadband Backend (Wilson et al. 2011) was configured in hybrid mode CFB 1M/64M, with both 2.048 GHz bands centered on 36.85 GHz. Two zoom bands were configured in the 64 MHz resolution intermediate frequency band (IF), covering the rest frequencies of the $4_1 \rightarrow 3_0$ E and $7_2 \rightarrow 8_1$ E transitions of methanol (marked in Figure 1), for which we adopted rest frequencies of 36.169265 and 37.703700 GHz, respectively (Müller et al. 2004). This resulted in a velocity range of -350 to 1200 km s^{-1} (barycentric) with a spectral resolutions of 0.26 km s^{-1} at 36.2 GHz. We have used the barycentric reference frame for all velocities reported in this paper. The FWHM of the primary beam of the ATCA antennas at 36.2 GHz is approximately 70 arcsec, and for an assumed distance of 3.7 Mpc to NGC 4945 this corresponds to a linear scale of 1200 pc. Our observations used a single pointing centered on the nucleus of

the galaxy and so are only sensitive to methanol maser emission within 600 pc of the center of the galaxy.

The data were reduced with MIRIAD using the standard techniques for ATCA 7 mm spectral line observations. Amplitude calibration was with respect to PKS B1934-648, and PKS B1253-055 was observed as the bandpass calibrator. The data were corrected for atmospheric opacity, and the absolute flux density calibration was estimated to be accurate to better than 30%. The observing strategy interleaved 10 minutes on-source with 2 minute observations of the phase calibrator (J1326-5256). The data were self-calibrated (phase and amplitude) using the continuum emission from the central region of NGC 4945. After self-calibration we used continuum subtraction (modeled using the spectral channels without maser emission) to isolate the spectral line and continuum emission components. The total duration on-source for NGC 4945 was 1.68 hr. Molecular line emission in NGC 4945 is observed between approximately 300 and 800 km s^{-1} (Ott et al. 2001), and the velocity range of our imaging covered the barycentric velocities between 200 and 1000 km s^{-1} , with a spectral resolution of 1 km s^{-1} and average rms noise of $\sim 2.2 \text{ mJy beam}^{-1}$ in each spectral channel. Positions were determined using the MIRIAD task imfit, which reports the peak value and location of a two-dimensional Gaussian fit for the emission in a given velocity plane within the spectral line cube.

3. Results

We detected emission from the 36.2 GHz methanol transition as well as 7 mm continuum emission toward NGC 4945 (see Table 1). The 37.7 GHz methanol transition was not detected from this source. We also looked for thermal emission from molecular lines within the bandpass of the recorded data and detected weak thermal emission from the HC_3N ($J = 4-3$) transition.

The 7 mm continuum emission is observed at the location of the galactic nucleus of NGC 4945 (location of the H_2O megamaser; Greenhill et al. 1997), while the 36.2 GHz methanol emission is observed to be offset by ~ 10 arcsec (see Figure 2), perpendicular from the position angle of the galactic disk ($43^\circ \pm 2^\circ$; Dahlem et al. 1993). We can more reliably measure offsets perpendicular to the disk, as the major axis of our elongated synthesized beam is parallel to the position angle of the galaxy. This angular offset corresponds to a linear projected separation of $174 \pm 14 \text{ pc}$ at an assumed distance of $3.7 \pm 0.3 \text{ Mpc}$ (Tully et al. 2013). The east–west array configuration combined with limited hour-angle range has made determination of an exact position for the methanol emission difficult due to a highly elongated synthesized beam. However, as the emission appears to compact, the position reported by imfit provides a suitable estimate until follow-up observations can be made with more complete uv coverage.

In contrast to the reasonably strong detection in the 36.2 GHz zoom, the 37.7 GHz has no detected emission to a level of around $2.5 \text{ mJy beam}^{-1}$. Similar to Ellingsen et al. (2014), the 37.7 GHz transition was only included as it could be simultaneously observed with the 36.2 GHz emission and was not expected to be detected due to its rarity in Galactic sources.

Table 1
36.2 GHz Methanol and Continuum Emission toward NGC 4945

	R.A. (J2000) (h m s)	Decl. (J2000) ($^{\circ}$ ' ")	Peak Flux (mJy)	Integrated Flux (mJy km s $^{-1}$)	Peak Velocity (km s $^{-1}$)	Velocity Range (km s $^{-1}$)
Methanol	13 05 28.093	-49 28 12.306	43.8	256 \pm 35	674	660–710
Continuum	13 05 27.467	-49 28 04.797	349	385 \pm 40

Note. Numbers in parenthesis indicate 3σ error in the value, and locations of emission are accurate to <0.4 arcsec.

4. Discussion

4.1. Masing Methanol in NGC 4945

This is the third time the 36.2 GHz methanol transition ($4_{-1} \rightarrow 3_0E$) has been observed in an extragalactic source (Ellingsen et al. 2014; Chen et al. 2015). In the two previous cases, the emission has been convincingly described as resulting from maser processes. It is important for us to justify that the 36.2 GHz methanol emission observed toward NGC 4945 is indeed maser emission, rather than the result of thermal processes. Thermal methanol has not previously been observed toward NGC 4945.

Narrow line widths are a prominent characteristic of class I methanol emission from within our Galaxy. The extragalactic 36.2 GHz emission observed from NGC 253 shares this property (~ 10 km s $^{-1}$; Ellingsen et al. 2014); however, the megamaser emission toward Arp 220 is significantly more broad (Chen et al. 2015). For NGC 4945 the 36.2 GHz methanol emission is spread over a velocity range of 50 km s $^{-1}$ (from 660 to 710 km s $^{-1}$), dominated by a narrow (FWHM line width of ~ 8 km s $^{-1}$) peak component at 674 km s $^{-1}$. There also appears to be a secondary component redshifted by approximately 30 km s $^{-1}$ that is much weaker (factor of four dimmer); however, it shares a similar line width. Therefore, we observe similar emission characteristics in NGC 4945 as displayed by the 36.2 GHz emission in NGC 253 (Ellingsen et al. 2014). In addition to the narrow line width, we observe no thermal emission associated with the location of the methanol emission, with the relatively weak thermal HC $_3$ N emission ($J = 4-3$) observed only toward the galactic nucleus. The velocity of this HC $_3$ N emission covers the same range that molecular line emission is observed from toward NGC 4945 (Ott et al. 2001). In contrast to the HC $_3$ N ($J = 4-3$) observations toward NGC 253 (Ellingsen et al. 2017a), in NGC 4945 there does not appear to be a close association with the 36.2 GHz methanol emission.

Considering the integrated intensity observed for the methanol emission of 0.258 Jy km s $^{-1}$, we determine an isotropic luminosity of 4.44×10^7 Jy km s $^{-1}$ kpc 2 . Compared with the 9.0×10^7 and 9.5×10^{11} Jy km s $^{-1}$ kpc 2 observed toward NGC 253 and Arp 220, respectively (note that there is a typographical error in Table 2 of Chen et al. 2015 and that the units for the integrated intensity are mJy km s $^{-1}$, not Jy km s $^{-1}$; Ellingsen et al. 2014; Chen et al. 2015). It should be noted that all luminosity values reported here include a factor of 4π , this was excluded from the value reported in Ellingsen et al. (2014). Voronkov et al. (2014) present data for a large number of Galactic 36.2 GHz methanol masers, and utilizing the data presented in their Table 3, along with distance estimates from Green & McClure-Griffiths (2011), we find 500 Jy km s $^{-1}$ kpc 2 to be a typical isotropic luminosity for this transition in Galactic high-mass star formation regions. If we consider 500 Jy km s $^{-1}$ kpc 2 representative of Galactic class I methanol

masers, the 36.2 GHz transition in NGC 4945 is approximately five orders of magnitude more luminous. This luminosity corresponds to an integrated intensity of 6.1×10^5 Jy km s $^{-1}$ at a distance of 8.5 kpc; therefore, this methanol emission in NGC 4945 is a factor of ~ 90 greater than the emission in the Milky Way CMZ (Yusef-Zadeh et al. 2013).

The narrow FWHM line width combined with an isotropic luminosity is comparable to that observed in NGC 253, and angular separation from any detected strong thermal emission provides a strong indication that the 36.2 GHz emission toward NGC 4945 is a maser. Future observations of NGC 4945 with better uv coverage will allow for more accurate determination of the size of the 36.2 GHz emission region. This more accurate imaging, combined with observations of thermal methanol in the central region of NGC 4945, will allow verification that this methanol emission is due to a maser process.

4.2. Properties of Methanol Maser Environment

H $_2$ O megamasers have been extensively observed toward NGC 4945 (in the 22, 183, and 321 GHz transitions); these megamasers are distributed within a circumnuclear accretion disk (<1 pc from nucleus) oriented parallel to the position angle of the galactic disk (Greenhill et al. 1997; Hagiwara et al. 2016; Humphreys et al. 2016; Pesce et al. 2016). In contrast, the methanol maser emission is significantly offset to the southeast of the galactic nucleus. This offset from the galactic center is consistent with the observed class I maser emission in Arp 220 and NGC 253 (Ellingsen et al. 2014; Chen et al. 2015). Ellingsen et al. (2014) observe offsets of 180 and 300 pc for the northeast and southwest components, respectively. Although the H $_2$ O maser emission observed in NGC 4945 is not physically associated with the 36.2 GHz maser emission, the redshifted components share an overlapping velocity range (Greenhill et al. 1997; Hagiwara et al. 2016; Humphreys et al. 2016; Pesce et al. 2016).

Detailed investigations of the molecular clouds in NGC 4945 have revealed an elliptical rotating molecular cloud complex extending approximately 400 pc with the major axis aligned with the galactic disk (Cunningham & Whiteoak 2005; Chou et al. 2007). The 36.2 GHz maser emission lies within the outer edge region of the CO and HCN circumnuclear molecular clouds, and there is no particular enhancement in the quiescent or dense gas molecular tracers at the location of the class I methanol maser emission (Cunningham & Whiteoak 2005; Chou et al. 2007). The 36.2 GHz maser emission is covered by the 540–750 km s $^{-1}$ velocity range of the 12 CO(2–1) and 13 CO(2–1) molecular gas (Chou et al. 2007). The associated molecular HCN emission is redshifted with respect to the systemic velocity of the galaxy; however, the velocity range of the emission, 570–618 km s $^{-1}$, falls short of the velocity covered by the class I methanol emission (Cunningham & Whiteoak 2005). Bendo et al. (2016) report free-free continuum and H42 α images of NGC 4945; however, this

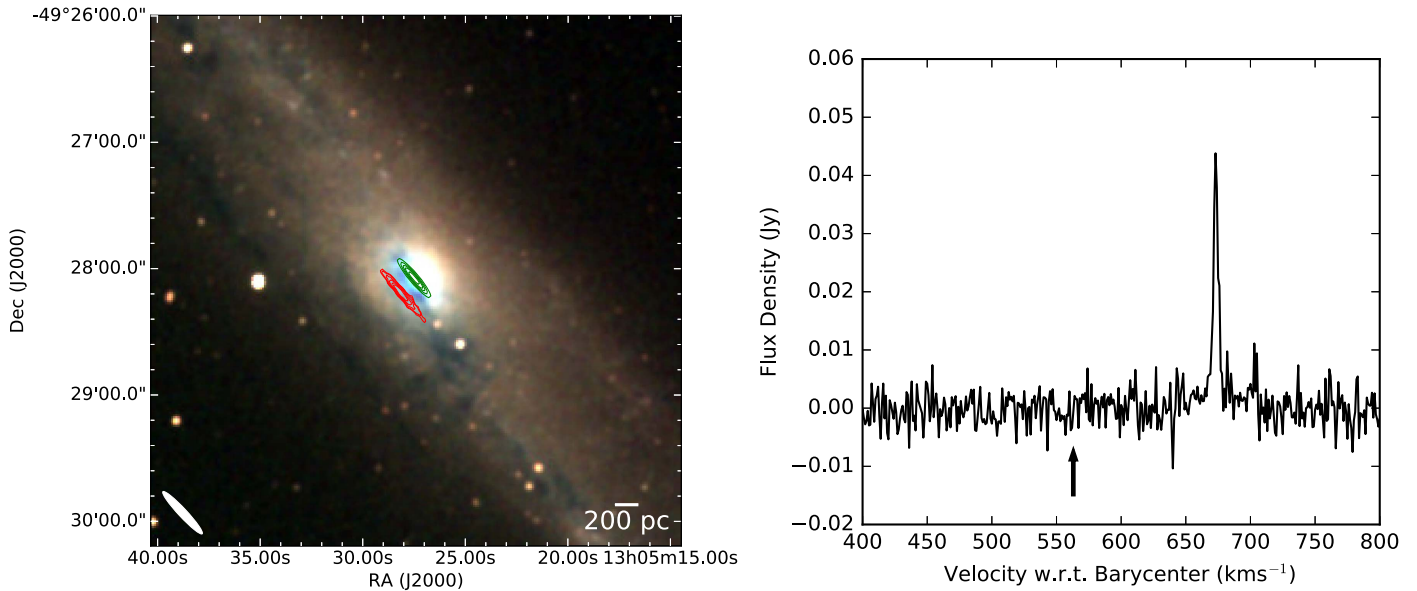


Figure 2. Left: 36.2 GHz emission methanol emission (red contours 45%, 50%, 60%, 70%, and 80% of the $256 \text{ mJy km s}^{-1} \text{ beam}^{-1}$) and the 7 mm continuum emission (green contours 15%, 30%, 45%, 60%, and 80% of the $385 \text{ mJy km s}^{-1} \text{ beam}^{-1}$) with a background 2MASS three-color image (J, H, and K bands in red, green, and blue, respectively). The white ellipse describes the synthesized beam size for our observations. Right: 36.2 GHz spectrum from the region of peak emission within our spectral line cube (imaged at 1 km s^{-1}). Vertical arrow indicates the systemic velocity of NGC 4945.

emission does not extend far enough southeast of the nucleus for the methanol maser to be associated.

The two regions of methanol maser emission in NGC 253 have recently been suggested as being associated with the inner interface of the galactic bar and CMZ (Ellingsen et al. 2017b). Like NGC 253, NGC 4945 is also classified as a barred-spiral galaxy; however, in comparison to NGC 253, the bar dynamics and molecular emission in NGC 4945 are relatively poorly studied, due to a combination of a more edge-on orientation and a more southern declination. The assumed bar position angle is 33° with an azimuth angle with respect to the plane of the galaxy of 40° (Ott et al. 2001). Analysis of CO(2-1) maps indicates that the bar could come as close as 100 pc to the galactic nucleus (Chou et al. 2007).

Observations of hydrogen fluoride (HF) absorption toward NGC 4945 by Monje et al. (2014) identify the possibility of molecular inflow toward the galactic center. This HF inflow has a velocity range of $560\text{--}720 \text{ km s}^{-1}$, and Monje et al. suggest an upper limit of $\sim 200 \text{ pc}$ on the radius of molecular inflow and maximum inflow velocity of 152 km s^{-1} . The observed class I maser emission falls both within this velocity range and is located closer than the upper limit stated for the radius of inflow. The majority of redshifted molecular gas in NGC 4945 is located northeast of the central region; therefore, the high redshift and southeastern position of the class I emission could be explained through molecular inflow. In addition, this would be consistent with the explanation that class I methanol emission is associated with large-scale molecular infall, as observed in NGC 253 (Ellingsen et al. 2017b).

The only extragalactic source for which there has been a detailed investigation of the relationship between class I methanol maser emission and other molecular lines is NGC 253 (Ellingsen et al. 2017b; Gorski et al. 2017). Hence, the reason why we observe 36.2 GHz class I methanol maser emission offset to the southeast of the center of NGC 4945 and not at other locations is largely speculation. Within the Milky Way, class II methanol masers are exclusively associated with

high-mass star formation (Breen et al. 2013), while class I masers (such as the 36.2 GHz transition) are found predominantly in high-mass star formation regions, with a handful of sources detected toward low-mass star formation regions and supernova–molecular cloud interaction regions. Breen et al. (2013) present a detailed discussion of current knowledge on the mechanisms by which gas-phase methanol is created and destroyed. Multiple lines of evidence suggest that methanol is formed on the surface of cold dust grains through hydrogenation of CO. Observations of 36.2 GHz methanol masers in NGC 253 and Arp 220 suggest that large-scale, low-velocity shocks are important, likely because they provide an efficient mechanism for releasing methanol from dust-grain mantles without dissociating it in the process. Once released into the gas phase, methanol is depleted relatively quickly through a combination of gas-phase chemistry and/or dissociation from shocks or external radiation fields. We suggest that the combination of cold molecular gas and low-velocity shocks (both on large scales) are the key requirements for the presence of a luminous class I methanol maser emission, such as is observed in NGC 4945. Under this hypothesis, the absence of other sites of 36.2 GHz methanol masers in NGC 4945 is likely because other regions where there are low-velocity shocks do not also contain sufficient cold molecular gas. In NGC 253, the regions where the class I methanol maser emission is observed show an enhancement in the HNC:SiO ratio (Meier et al. 2015; Ellingsen et al. 2017b). This is thought to reflect the low-velocity shocks compared to more energetic shocks in molecular gas. Therefore, we predict that observations of these two molecular tracers toward NGC 4945 will likely show an enhancement of HNC relative to SiO at the methanol maser location compared to the rest of the galaxy.

Although our sample size is not sufficiently large to perform any detailed analysis of trends that identify likely candidates for future searches of class I methanol emission, understanding the similarities between all known host galaxies may help future searches. This is the second barred-spiral starburst





galaxy with class I emission potentially associated with molecular inflow. Therefore, we suggest targeting future searches for 36.2 GHz emission in galaxies with similar properties.

5. Conclusion

We present 36.2 GHz ($4_{-1} \rightarrow 3_0E$) imaging results of the starburst galaxy NGC 4945. A region of 36.2 GHz methanol emission is observed, offset from the galactic nucleus by 174 pc, while emission from the 37.7 GHz transition was not detected. The lack of strong observed thermal emission (from this same offset region) combined with narrow line width and high isotropic luminosity indicate that this region is a likely class I maser. The maser emission may be associated with molecular inflow, which is observed in HF absorption. If this is the case, it would fit with the explanations of similar emission in NGC 253. This is the third detection of 36.2 GHz masers in any extragalactic source and the second within a barred starburst galaxy. As our sample size increases it will become easier to identify factors that make galaxies appropriate hosts for class I methanol masers and will allow higher success rates in targeted searches.

The Australia Telescope Compact Array is part of the Australia Telescope National Facility, which is funded by the Commonwealth of Australia for operation as a National Facility managed by CSIRO. This research has made use of NASA's Astrophysics Data System Abstract Service. This research also utilized APLPY, an open-source plotting package for PYTHON hosted at <http://aplp.github.com>. This research made use of Astropy, a community-developed core Python package for Astronomy (Astropy Collaboration et al. 2013).

ORCID iDs

Tiege P McCarthy  <https://orcid.org/0000-0001-9525-7981>
 Simon P. Ellingsen  <https://orcid.org/0000-0002-1363-5457>
 Shari L. Breen  <https://orcid.org/0000-0002-4047-0002>
 Hai-hua Qiao  <https://orcid.org/0000-0003-0196-4701>

References

- Astropy Collaboration, Robitaille, T. P., Tollerud, E. J., et al. 2013, *A&A*, **558**, A33
- Bendo, G. J., Henkel, C., D'Cruze, M. J., et al. 2016, *MNRAS*, **463**, 252
- Breen, S. L., Caswell, J. L., Ellingsen, S. P., & Phillips, C. J. 2010, *MNRAS*, **406**, 1487
- Breen, S. L., Ellingsen, S. P., Contreras, Y., et al. 2013, *MNRAS*, **435**, 524
- Breen, S. L., Fuller, G. A., Caswell, J. L., et al. 2015, *MNRAS*, **450**, 4109
- Caswell, J. L., Fuller, G. A., Green, J. A., et al. 2010, *MNRAS*, **404**, 1029
- Caswell, J. L., Fuller, G. A., Green, J. A., et al. 2011, *MNRAS*, **417**, 1964
- Chen, X., Ellingsen, S. P., Baan, W. A., et al. 2015, *ApJL*, **800**, L2
- Chou, R. C. Y., Peck, A. B., Lim, J., et al. 2007, *ApJ*, **670**, 116
- Cunningham, M. R., & Whiteoak, J. B. 2005, *MNRAS*, **364**, 37
- Cyganowski, C. J., Brogan, C. L., Hunter, T. R., & Churchwell, E. 2009, *ApJ*, **702**, 1615
- Cyganowski, C. J., Brogan, C. L., Hunter, T. R., et al. 2012, *ApJL*, **760**, L20
- Dahlem, M., Golla, G., Whiteoak, J. B., et al. 1993, *A&A*, **270**, 29
- Done, C., Madejski, G. M., & Smith, D. A. 1996, *ApJL*, **463**, L63
- Ellingsen, S. P. 2006, *ApJ*, **638**, 241
- Ellingsen, S. P., Breen, S. L., Caswell, J. L., Quinn, L. J., & Fuller, G. A. 2010, *MNRAS*, **404**, 779
- Ellingsen, S. P., Chen, X., Breen, S. L., & Qiao, H.-h. 2017a, *ApJL*, **841**, L14
- Ellingsen, S. P., Chen, X., Breen, S. L., & Qiao, H.-H. 2017b, *MNRAS*, **472**, 604
- Ellingsen, S. P., Chen, X., Qiao, H.-H., et al. 2014, *ApJL*, **790**, L28
- Ellingsen, S. P., Shabala, S. S., & Kurtz, S. E. 2005, *MNRAS*, **357**, 1003
- Gorski, M., Ott, J., Rand, R., et al. 2017, *ApJ*, **842**, 124
- Green, J. A., & McClure-Griffiths, N. M. 2011, *MNRAS*, **417**, 2500
- Green, J. A., Caswell, J. L., Fuller, G. A., et al. 2008, *MNRAS*, **385**, 948
- Green, J. A., Caswell, J. L., Fuller, G. A., et al. 2010, *MNRAS*, **409**, 913
- Green, J. A., Caswell, J. L., Fuller, G. A., et al. 2012, *MNRAS*, **420**, 3108
- Green, J. A., Breen, S. L., Fuller, G. A., et al. 2017, *MNRAS*, **469**, 1383
- Greenhill, L. J., Moran, J. M., & Herrnstein, J. R. 1997, *ApJL*, **481**, L23
- Hagiwara, Y., Horiuchi, S., Doi, A., Miyoshi, M., & Edwards, P. G. 2016, *ApJ*, **827**, 69
- Haschick, A. D., & Baan, W. A. 1989, *ApJ*, **339**, 949
- Humphreys, E. M. L., Vlemmings, W. H. T., Impellizzeri, C. M. V., et al. 2016, *A&A*, **592**, L13
- Kalenskii, S. V., Johansson, L. E. B., Bergman, P., et al. 2010, *MNRAS*, **405**, 613
- Kurtz, S., Hofner, P., & Álvarez, C. V. 2004, *ApJS*, **155**, 149
- Licquia, T. C., & Newman, J. A. 2015, *ApJ*, **806**, 96
- Marconi, A., Oliva, E., van der Werf, P. P., et al. 2000, *A&A*, **357**, 24
- Meier, D. S., Walter, F., Bolatto, A. D., et al. 2015, *ApJ*, **801**, 63
- Monje, R. R., Lord, S., Falgarone, E., et al. 2014, *ApJ*, **785**, 22
- Müller, H. S. P., Menten, K. M., & Mäder, H. 2004, *A&A*, **428**, 1019
- Müller, H. S. P., Thorwirth, S., Roth, D. A., & Winnewisser, G. 2001, *A&A*, **370**, L49
- Ott, M., Whiteoak, J. B., Henkel, C., & Wielebinski, R. 2001, *A&A*, **372**, 463
- Pérez-Beaupuits, J. P., Spoon, H. W. W., Spaans, M., & Smith, J. D. 2011, *A&A*, **533**, A56
- Pesce, D. W., Braatz, J. A., & Impellizzeri, C. M. V. 2016, *ApJ*, **827**, 68
- Pihlström, Y. M., Sjouwerman, L. O., Frail, D. A., et al. 2014, *AJ*, **147**, 73
- Sjouwerman, L. O., Murray, C. E., Pihlström, Y. M., Fish, V. L., & Araya, E. D. 2010, *ApJL*, **724**, L158
- Spoon, H. W. W., Koornneef, J., Moorwood, A. F. M., Lutz, D., & Tielens, A. G. G. M. 2000, *A&A*, **357**, 898
- Spoon, H. W. W., Moorwood, A. F. M., Pontoppidan, K. M., et al. 2003, *A&A*, **402**, 499
- Tully, R. B., Courtois, H. M., Dolphin, A. E., et al. 2013, *AJ*, **146**, 86
- Voronkov, M. A., Caswell, J. L., Ellingsen, S. P., Green, J. A., & Breen, S. L. 2014, *MNRAS*, **439**, 2584
- Voronkov, M. A., Caswell, J. L., Ellingsen, S. P., & Sobolev, A. M. 2010, *MNRAS*, **405**, 2471
- Wang, J., Zhang, J., Gao, Y., et al. 2014, *NatCo*, **5**, 5449
- Wilson, W. E., Ferris, R. H., Axtens, P., et al. 2011, *MNRAS*, **416**, 832
- Yusef-Zadeh, F., Cotton, W., Viti, S., Wardle, M., & Royster, M. 2013, *ApJL*, **764**, L19